Heat treatment of a Beta-Ti21S alloy produced by additive manufacturing

L. Emanuelli, V. Tonon, M. Pellizzari, G. Valsecchi, C. Lora

Metastable β-Ti alloys are a class of heat-treatable materials increasing research interest nowadays. Their mechanical properties make them very suitable for high-end applications, such as racing and aerospace. In this study, the heat treatment behaviour of β-21S (Timetal 21S) fabricated by laser powder bed fusion (L-PBF) was investigated, to evaluate its influence on microstructure and mechanical properties. Solution heat treatment (SHT) at 930 °C x for 30 min allowed an equiaxed microstructure with no massive grain coarsening. Artificial ageing (AA) at 590 °C x 8h following SHT resulted in higher strength, compared to that achieved by direct ageing, and in α precipitation shifted to higher temperatures with a triangular arrangement. The suitability of two different direct ageing treatments, namely AA (590°C for 8h), and double ageing (DA) at 690°C for 8h plus 650°C for 8h, could be confirmed for the AM alloy. Both treatments provided strength values comparable to literature findings but also in an incredibly high elongation at break. AA provided a yield strength of about 1200 MPa and preserved the elongation at break of the as-built material (21%). On the other hand, the outstanding fracture elongation after DA (34%) led to a slightly lower strength (970 MPa). On the other hand, SHT+AA resulted in a higher strength (1286MPa) but also in very limited ductility (7%) due to the grain boundary precipitation of alpha phase.

KEYWORDS: METASTABLE BETA TITANIUM ALLOYS, TI-21S, HEAT TREATMENTS , LASER POWDER BED FUSION, ADDITIVE MANUFACTURING

INTRODUCTION

Titanium alloys, based on Ti with addition of elements such us Al, V, Fe and Mo, are of good interest in aerospace, automotive, military, medical, sporting and other applications where low-density (around 4.51 g/cm3) with high strength and high corrosion resistance are of primary importance [1,2]. In addition, their excellent biocompatibility and low elastic modulus compared with the other metallic biomaterials make them the far most used material in the orthodontic and orthopedic fields [3–5]. Titanium alloys are divided in three different classes, α, α+β, and β phase with further subdivision into near α and metastable β alloys depending on the alloying elements used to stabilize the two allotropic phases of Ti, namely hexagonal close-packed (hcp) α-phase and the body-centered cubic (bcc) β-phase. Indeed, alloying elements could be divided into α-stabilizers, namely Al, O, N and C, which extend the α field to higher temperatures

Lorena Emanuelli,
Vassili Tonon,
Massimo Pellizzari
University of Trento

Giorgio Valsecchi
TAV

Carlo Lora
SISMA SpA

and β-stabilizers, such as Mo, V, Ta, Nb, Fe, Mn, Cr, Co, Ni, Cu, Si and H, which decrease the β-transus temperature [2,6]. β-Ti alloys have progressively replaced iron and nickel based alloys in the aerospace industry thanks to the unique strength to weight ratio, excellent temperature resistance up to around 600°C and high hardenability [7,8]. Furthermore, they are having a growing interest in for biomedical applications thanks to the lower elastic modulus achieved with the β microstructure compared to the common metallic biomaterials [8]. A subgroup of the β-alloys is given by the metastable β-alloys which can be composed with a small volume fractions of other phases such as α, martensitic phases or ω-phase depending on composition and thermo-mechanical processing [4,7]. Among this group of β-alloys, β-21S, which is characterized by a chemical composition of Ti-15Mo-3Nb-3Al-0.2Si (wt.%), is of good interest in a variety of applications where high temperature strength, creep resistance, thermal stability and oxidation resistance are required [9,10]. With the aim of produce β-21S high complexity components, additive manufacturing (AM) technologies are gaining increasing interest thanks to the possibility to decrease the time and cost of production and high design freedom and good tolerance [11]. One of the most used AM techniques is the laser powder bed fusion (L-PBF) offering the best dimensional precision and accuracy [12]. Pellizzari et. Al. [10] have demonstrated the achievement of interesting properties for biomedical applications, namely a low elastic modulus e good mechanical properties, by producing β-21S alloys via L-PBF. Nevertheless, this alloy results in a promising candidate for strength applications thanks to precipitation hardening achieved through specific heat treatments. Typical heat treatment of cast and wrought Ti21S alloy involves solution heat treatment (SHT) above the β-transus temperature to recrystallize and recover anisotropy and guarantee homogenous response to the following artificial aging (AA) between 500 and 700°C [13]. Aging is aimed at strengthening the material through the precipitation of α phase inside grains. Depending on the required mechanical properties, aging at 500°C is used to achieve higher strength to toughness/ductility ratios; differently, aging at higher temperature leads to a recovering of the ductility at the expense of strength [14,15]. Two other heat treatments are commercially diffused for Ti21S, namely direct aging (AA) at around 590°C for 8h for low temperature applications and double aging (DA) at 690°C for 8h and 650°C for 8h when higher thermal stability is required [13].

In this work, heat treatment response of β-21S produced by L-PBF was investigated. Three different heat treatments (HTs), namely direct aging (AA), solution treatment followed by aging (STA) and double aging (DA) were performed. The effects of the different heat treatments on the microstructure, mechanical properties and residual stresses were evaluated.

MATERIALS AND METHODS

A β-Ti21S pre-alloyed powder (GKN Hoeganaes Corporation, USA, D_{10}=25 μm, D_{50}=41 μm, D_{90}=60 μm) was used. Dog-bone (ASTM E8M) samples were 3D printed with the main axis parallel to the building direction (BD) using a L-PBF machine model SISMA MYSINT100 on a platform of 100 mm in Ar atmosphere. A laser spot of 55 μm, a power of 200W, a volume energy density comprised between 40 and 90 J/mm^3 and a 90° scanning strategy were used. Heat treatments were carried out in a vacuum furnace, equipped with an all-metal molybdenum hot zone. Samples were placed horizontally inside the furnace, using nickel-based alloy fixtures. Once established high vacuum (1E-5/1E-6 mbar range of pressure), samples were heated 10°C/min to the selected temperature. After soaking, the samples were cooled to room temperature using pressurized argon at 1.5 bar for the aging treatments and pressurized argon at 6 bar for the solution heat treatment. During double aging (DA), samples were furnaced cooled (~ 1.3°C/min) from the Aging 1 temperature (690°C) to Aging 2 temperature (650°C). Details of the different heat treatments are summarized in Tab. 1.

Tab.1 - Heat treatments of tensile specimens. if not specified, heating rate is equal to 10°C/min and cooling rate of 30 °C/min

HEAT TREATMENT DETAILS			
HTs	**Solution**	**Aging 1**	**Aging 2**
AA	-	590°C for 8h	
STA	930°C for 30 min RT* in 6 min	590°C for 8h	
DA	-	690°C for 8h FC** until 650°C	650°C for 8h

* RT room temperature (RT); ** FC Furnace cooling.

Tensile tests were carried out according to ASTM E8 at RT, with a strain rate of 1 mm/min and using an extensometer with a 12.5 mm gauge length to evaluate the elastic region of the curves. After sandblasting, three samples for each condition were tested. The microstructural characterization of as-built (AB) and HTs samples was carried out by light optical (LOM) and scanning electron microscopy (SEM) after proper metallographic preparation and chemical etching with Kroll's reagent [16]. Fractographic analysis on the AB and HTs samples after tensile testing was performed by means of SEM. Cantilever tests, using the geometry reported by C. Pauzon et al. [17], were conducted to evaluate the accumulated residual stresses due to L-PBF, on the AB and HTs samples. Specific point of the cantilever (P1, P2 etc.) were measured with Coordinate Measuring Machine (CMM) Global DEA 07-07-07 equipped with a Renishaw SP600M scanning head after the detachment, by means of Electrical Discharge Machining (EDM), of the thin supports that connect the cantilever with the platform.

RESULTS AND DISCUSSION

Microstructural analysis

As built microstructure shown in Fig. 1a clearly evidences the 90° scanning strategy used during L-PBF. A fully dense material and a columnar β grain structure oriented along the building direction is observed (Fig. 1b). In addition, traces of melting pools and the epitaxial growth of β grain which takes place along the heat flow direction are detected. The partial remelting of previously consolidated layers promotes the extension of epitaxial growth of β grain up several millimeters in length with a thickness of around 10 μm. The solidification structure, namely the grain orientation, is influenced by the local heat flow direction, which is almost parallel to the building direction [10,18].

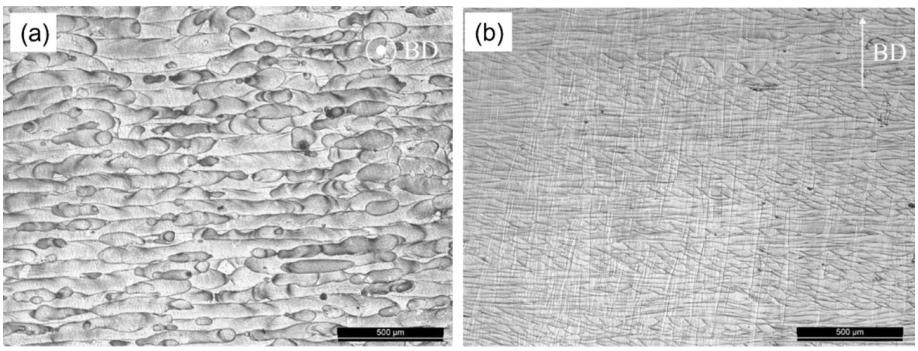

Fig.1 - AB microstructure a) perpendicular and b) parallel to the BD

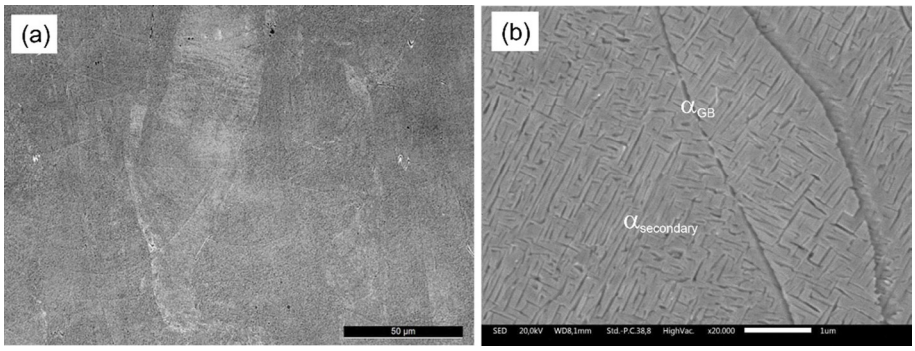

Fig.2 - a) LOM micrograph and b) high magnification SEM micrograph of the AA sample

After AA, the solidification microstructure and the melting pools are still visible. Indeed, the AA is not able to remove the solidification microstructure and the anisotropy introduced by L-PBF. Some α colonies at the β grain boundaries (α_{GB}) seems to be present, even though this should be confirmed by higher resolution techniques. SEM micrograph (Fig. 2b) highlights presence of α phase with a banded and Widmanstätten morphology of a size lower than 1 μm inside β grains confirming a predominant intragranular precipitation along specific directions. LOM and SEM micrographs of DA treatment are reported in Fig. 3.

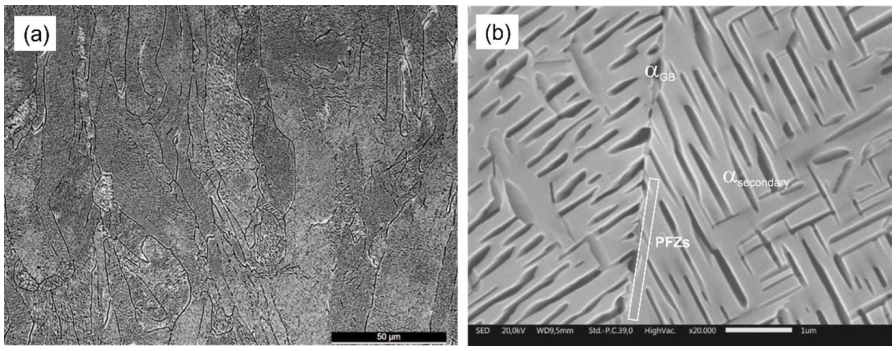

Fig.3 - a) LOM and b) SEM micrographs of DA sample

The solidification microstructure characterized by elongated grains is preserved as in case of AA but only few melting pools boundaries are still visible (Fig. 3a). Higher amount of α_{GB} respect to AA is observed in SEM micrograph (Fig. 3b). Near the α_{GB} a thin layer of β-phase without precipitates is formed called precipitates free zones (PFZs). These zones increase the ductility of the alloy [19]. Secondary α precipitates inside the β grains with a specific orientation size of around 1-2 μm. LOM and SEM micrographs achieved after STA (930°C for 30min + 590°C for 8h) treatment are shown in Fig. 4.

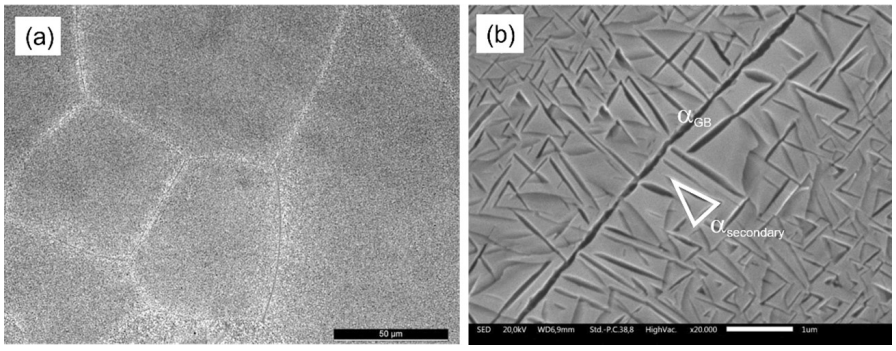

Fig.4 - LOM and b) SEM micrographs of STA sample.

The solution heat treatment (SHT) promotes the recrystallization deleting the columnar structure achieved by L-PBF and creating equiaxed grains about 80 μm in size. The high temperature reached during SHT then promotes a significant microstructural isotropy recovery. Thanks to homogenization, the precipitation of secondary α occurs with a peculiar triangular α lamellae arrangement (Fig. 4b). A thin layer of α_{GB} is observed highlighting a poor quench after ST.

Tensile tests

The nominal tensile stress-strain curves of AB and heat treated specimens are reported in Fig. 5a.

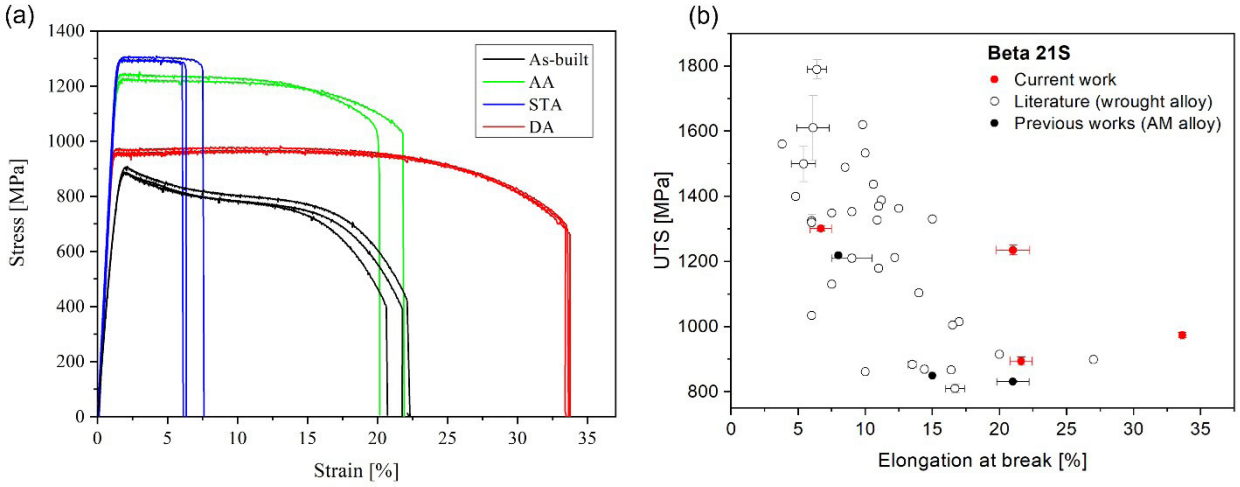

Fig.5 - a) Nominal tensile stress-strain curve of β-Ti21S obtained by L-PBF in AB condition and after three different HTs. b) Comparison between the mechanical properties achieved in this work and those reported in literature for the same wrought alloy and previous works on additively manufactured Ti-21S.

The corresponding mechanical properties are summarized in Tab. 2. The AB material shows an elastic modulus of 64 GPa, a fracture elongation around 22%, a yield strength of 804 MPa, and a UTS of 894MPa. Looking the AB stress-strain curve (Fig. 5a), after the first part related to elastic region, a very intense work softening highlighting by a marked stress drop it is observed. This behavior is ascribed to the planar inhomogeneous plastic flow enhanced by an increased localized adiabatic temperature [20,21].

Tab.2 -Mechanical properties of β-Ti21S obtained by L-PBF in AB condition and after different HTs.

MECHANICAL PROPERTIES					
	E (GPa)	σy [MPa]	UTS [MPa]	εR [%]	mHV0.1
AB	64 ± 1	804 ± 29	894 ± 13	21.6 ± 0.8	299 ± 2
AA	96 ± 1	1208 ± 19	1235 ± 15	21.0 ± 1.2	376 ± 4
DA	96 ± 0	951 ± 11	974 ± 8	33.6 ± 0.1	310 ± 4
STA	96 ± 0	1286 ± 6	1301 ± 7	6.7 ± 0.8	377 ± 2

Heat treated samples show equal elastic modulus of 96GPa that is higher respect to the one of AB. This is ascribed to the precipitation of α phase that occurs in all three HTs as demonstrated through previous microstructural investigation. Comparing the HTs stress-strain curves with the one of AB, after yielding the strain softening observed in AB is disappeared and is replaced by strain hardening leading to a material with a more predictable and controllable behavior. Direct aging (AA) leads to an increase in the strength with no significant variation in break elongation thanks to the precipitation of fine secondary alpha inside the β grains. Considering STA, the

higher strength respect to AA is accompanied by a marked drop in ductility, to be ascribed to the extended and rather continuous grain boundary precipitation of brittle α phase [22]. In case of DA thermal treatment, outstanding fracture elongation (34%) with slightly lower strength (970 MPa) respect to the other HTs and higher in comparison with AB is observed. The enhanced ductility compared with AA can be reasonably attributed to the formation of PFZs near the α_{GB} (Fig. 4b). Differently, the slight decrease in strength respect to AA is due to the coarsening of secondary α [23].

Comparison between the mechanical properties achieved in this work and those reported in literature for the same wrought alloy are shown in Fig. 5b. Except for the STA, the samples AB, AA and DA provide outstanding ductility near the highest values of wrought alloy and highest then the values refer to alloy obtained by means of AM. In terms of strength, highest values are obtained compared with other works on β-Ti21S AM alloy in all different conditions [9,10,13,21,24,25].

SEM fracture surface micrographs are reported in Fig. 6.

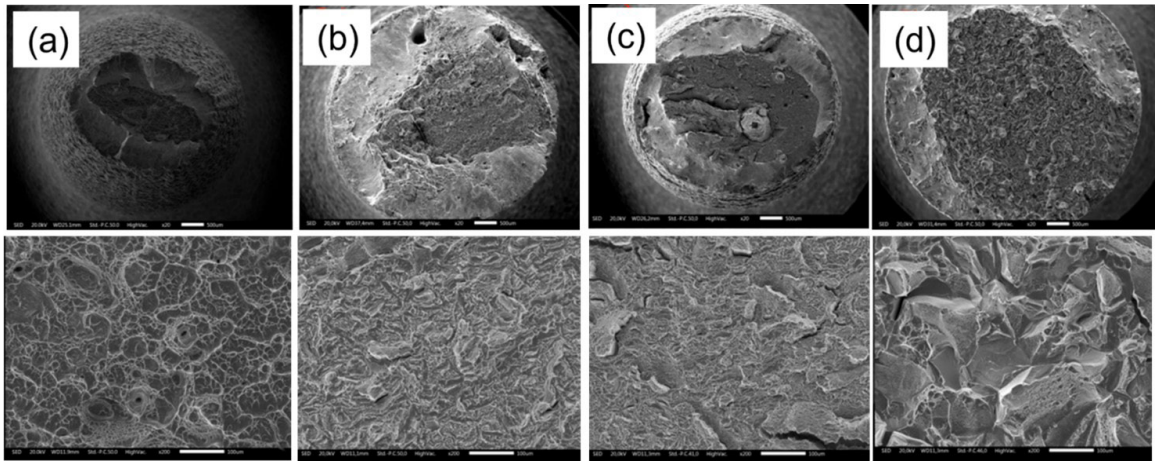

Fig.6 - Fracture surfaces of tensile specimens at low and high magnification of a) AB, b) AA, c) DA and d) STA.

A ductile fracture surface highlighted by extended presence of dimples is observed in AB, AA and DA samples (Fig. 6a, b and c) differently from the STA samples where an intergranular fracture is highlighted (Fig. 6d). This is in agreement with the stress-strain curves that show a ductile behavior in case of AB, AA and DA and a drastic drop of the ductility in case of STA.

Cantilever test

The accumulated residual stresses due to L-PBF, on the AB and HTs samples are measured by means of cantilever test. The vertical displacement curves of the cantilever samples after detachment of the supports of the AB, AA, DA and STA specimens are shown in Fig. 7.

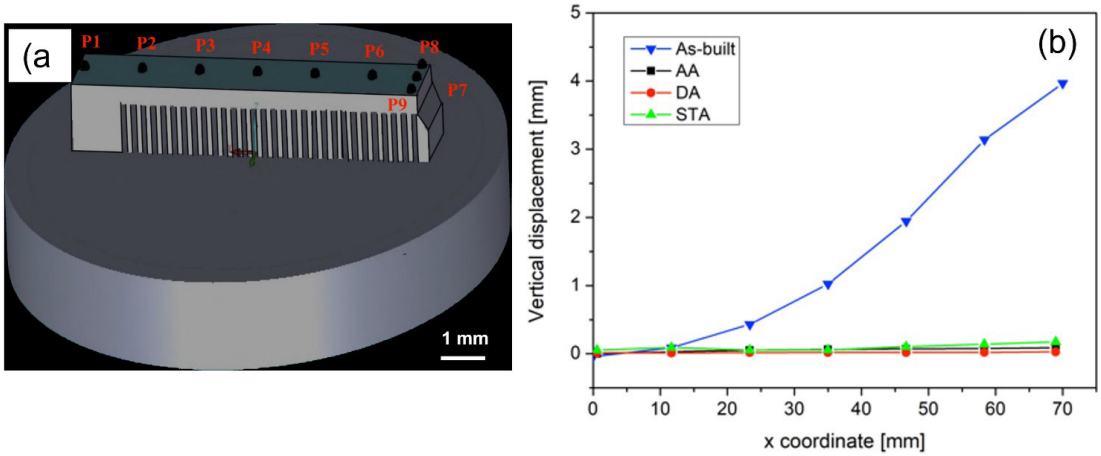

Fig.7 - a) Cantilever sample on the building platform with position of vertical displacement measurements. b)Vertical displacement of specific point along the cantilever sample after support removal.

A evident vertical deflection after removal of the support is observed in case of AB since the release of stresses introduced by L-PBF. Differently, all HTs provide negligible vertical deflection thanks to the stress relieving, without particular differences for different HTs.

CONCLUSIONS

In this study, the heat treatment behaviour of β-Ti21S fabricated by L-PBF was investigated, to evaluate its influence on microstructure and mechanical properties. In details, direct aging (AA), double aging (DA) and solution heat treatment followed by artificial aging (STA) were carried out on dog-bone specimens. The main conclusion could be summarized as follows.

- Direct artificial aging of AB alloy at 590 °C x 8 h shows an increase in strength with no significant variation in break elongation thanks to the precipitation of fine secondary Widmannstätten-α platelets inside the β grains;
- Double aging treatment at 690 °C x 8 h + 650 °C x 8h permits to achieve outstanding fracture elongation (34%) due to the formation of PFZs and slightly lower strength respect to the other HTs involving ageing at lower temperature, due to coarsening of secondary α The enhanced ductility compared with the AA could be attributed to the formation of PFZs.
- Solution heat treatment (SHT) at 930 °C x for 30 min promotes recrystallization of β grains deleting the columnar structure produced by L-PBF and allowed an equiaxed microstructure with no massive grain growth. Following artificial ageing (AA) at 590 °C x 8h resulted in higher strength, compared to that achieved by direct ageing, since the formation of secondary α with a triangular arrangement. The high ductility drop could be ascribed to the grain boundary precipitation of α phase that acts as a barrier to dislocation slip.
- Cantilever test confirmed the complete removal of residual stresses for all the three HTs.

In conclusion, direct ageing revealed itself a valid solution in providing appropriate mechanical properties and dimensional stability on the expenses of isotropy that can be recovered only by solution annealing.

Funding

This work is part of the project N. 2020.0042 - ID 50430, "Produzione additiva di protesi ortopediche a strut-tura trabecolare in Ti-beta" funded by Fondazione Cariverona.

Conflict of interest

The authors declare that they have no known financial interests or personal relationships that could have appeared to influence the work reported in this paper.

REFERENCES

[1] F.H. Sam Froes, M. Qian, M. Niinomi, Titanium for consumer applications: Real world use of titanium, Titan. Consum. Appl. Real-World Use Titan. (2019) 1–349. https://doi.org/10.1016/C2017-0-03513-9.
[2] Dr. Christoph Leyens, Dr. Manfred Peters, Titanium and Titanium Alloys, Titan. Titan. Alloy. (2003). https://doi.org/10.1002/3527602119.
[3] C. Sai Pitchi, A. Priyadarshini, G. Sana, S. Kumar Reddy Narala, A review on alloy composition and synthesis of b-Titanium alloys for biomedical applications, (2020). https://doi.org/10.1016/j.matpr.2020.02.468.
[4] R.P. Kolli, A. Devaraj, A review of metastable beta titanium alloys, Metals (Basel). 8 (2018). https://doi.org/10.3390/MET8070506.
[5] C.S. Pitchi, A. Priyadarshini, G. Sana, S.K.R. Narala, A review on alloy composition and synthesis of β-Titanium alloys for biomedical applications, Mater. Today Proc. 26 (2020) 3297–3304. https://doi.org/10.1016/J.MATPR.2020.02.468.
[6] J.C. Colombo-Pulgarín, C.A. Biffi, M. Vedani, D. Celentano, A. Sánchez-Egea, A.D. Boccardo, J.P. Ponthot, Beta Titanium Alloys Processed By Laser Powder Bed Fusion: A Review, J. Mater. Eng. Perform. 2021 309. 30 (2021) 6365–6388. https://doi.org/10.1007/S11665-021-05800-6.
[7] R.R. Boyer, Aerospace applications of beta titanium alloys, JOM. 46 (1994) 20–23. https://doi.org/10.1007/BF03220743/METRICS.
[8] S. Rajan Soundararajan, J. Vishnu, G. Manivasagam, N. Rao Muktinutalapati, Processing of Beta Titanium Alloys for Aerospace and Biomedical Applications, Titan. Alloy. - Nov. Asp. Their Process. [Working Title]. (2018). https://doi.org/10.5772/INTECHOPEN.81899.
[9] M.A. Macias-Sifuentes, C. Xu, O. Sanchez-Mata, S.Y. Kwon, S.E. Atabay, J.A. Muñiz-Lerma, M. Brochu, Microstructure and mechanical properties of β-21S Ti alloy fabricated through laser powder bed fusion, Prog. Addit. Manuf. 6 (2021) 417–430. https://doi.org/10.1007/S40964-021-00181-7/FIGURES/16.
[10] M. Pellizzari, A. Jam, M. Tschon, M. Fini, C. Lora, M. Benedetti, A 3D-printed ultra-low young's modulus β-Ti alloy for biomedical applications, Materials (Basel). 13 (2020) 1–16. https://doi.org/10.3390/ma13122792.
[11] J. Pelleg, Additive and Traditionally Manufactured Components: A Comparative Analysis of Mechanical Properties, Addit. Tradit. Manuf. Components A Comp. Anal. Mech. Prop. (2020) 1–642. https://doi.org/10.1016/C2019-0-04180-5.

[12] J. V. Gordon, S.P. Narra, R.W. Cunningham, H. Liu, H. Chen, R.M. Suter, J.L. Beuth, A.D. Rollett, Defect structure process maps for laser powder bed fusion additive manufacturing, Addit. Manuf. 36 (2020). https://doi.org/10.1016/J.ADDMA.2020.101552.

[13] J.D. Cotton, R.D. Briggs, R.R. Boyer, S. Tamirisakandala, P. Russo, N. Shchetnikov, J.C. Fanning, State of the Art in Beta Titanium Alloys for Airframe Applications, JOM. 67 (2015) 1281–1303. https://doi.org/10.1007/S11837-015-1442-4/FIGURES/25.

[14] T.W. Xu, H.C. Kou, J.S. Li, F.S. Zhang, Y. Feng, Effect of Phase Transformation Conditions on the Microstructure and Tensile Properties of Ti-3Al-15Mo-3Nb-0.2Si Alloy, J. Mater. Eng. Perform. 24 (2015) 3018–3025. https://doi.org/10.1007/S11665-015-1583-1/FIGURES/9.

[15] S. Rajan Soundararajan, J. Vishnu, G. Manivasagam, N. Rao Muktinutalapati, Heat Treatment of Metastable Beta Titanium Alloys, Weld. - Mod. Top. (2021). https://doi.org/10.5772/INTECHOPEN.92301.

[16] S. Practice, Standard Practice for Microetching Metals and Alloys ASTM E-407, 07 (2016) 1–22. https://doi.org/10.1520/E0407-07R15E01.2.

[17] C. Pauzon, T. Mishurova, S. Evsevleev, S. Dubiez-Le Goff, S. Murugesan, G. Bruno, E. Hryha, Residual stresses and porosity in Ti-6Al-4V produced by laser powder bed fusion as a function of process atmosphere and component design, Addit. Manuf. 47 (2021) 102340. https://doi.org/10.1016/J.ADDMA.2021.102340.

[18] A. Jam, A. du Plessis, C. Lora, S. Raghavendra, M. Pellizzari, M. Benedetti, Manufacturability of lattice structures fabricated by laser powder bed fusion: A novel biomedical application of the beta Ti-21S alloy, Addit. Manuf. 50 (2022) 102556. https://doi.org/10.1016/J.ADDMA.2021.102556.

[19] G. Lütjering, J. Albrecht, C. Sauer, T. Krull, The influence of soft, precipitate-free zones at grain boundaries in Ti and Al alloys on their fatigue and fracture behavior, Mater. Sci. Eng. A. 468–470 (2007) 201–209. https://doi.org/10.1016/J.MSEA.2006.07.168

TORNA ALL'INDICE >